The thermal stability of highly filled high-density polyethylene quaternary composites: interactive effects and improved measures

WD Viljoen[a,*], FJWJ Labuschagné[a]

[a] *Institute of Applied Materials, Department of Chemical Engineering, University of Pretoria, Private Bag X20, Hatfield 0028, South Africa*

Abstract

A range of formulations – consisting of high-density polyethylene, surface-coated calcium carbonate, masterbatched carbon black and a stabiliser package – were compared in terms of their thermal stability through the use of several techniques and measures. Notably, calcium carbonate loadings of up to 60 wt% were investigated. The formulations were designed to be I- and D-optimal, based on a quadratic Scheffé polynomial model. Novel and established measures for the thermal stability of the materials were compared, based on data generated using techniques for the determination of oxidative induction time and for studies by time-sweep oscillatory rheometry. For ease of comparison, all tests were performed in air. Fourier-transform infrared spectroscopy was performed on the materials subjected to time-sweep oscillatory rheometry, to ascertain the locality and modes of degradation. Variable effects were found, depending on the technique used. Broadly, strong primary effects were found: positive in the cases of the carbon black and stabiliser pack, negative in the case of calcium carbonate. The latter, however, was offset by the highly synergistic interaction of calcium carbonate with the stabiliser pack. Time-sweep oscillatory rheometry was shown to be a promising method, with it yielding high-quality, comparable results when interpreted using a novel measure.

Keywords: experimental design, high-density polyethylene, highly filled composites, oxidative induction time, thermal degradation, time-sweep rheometry

1. Introduction

High-density polyethylene (HDPE) is one of the most common commodity polymers in the world, with uses spanning from bottles and children's toys to pipes and geomembranes [1]. This is due to its unique set of properties,

*Corresponding author
Email address: wd.viljoen@tuks.co.za (WD Viljoen)

including a high strength to weight ratio, excellent chemical resistance, low cost and straightforward processing. Contra to this, however, it is subject to creep, high shrinkage and UV degradation (as a result of remnants of the transition metals used to catalyse its polymerisation) [2, 3, 4].

Typically, polymers are modified through the addition of additives to reduce their cost, modify their properties or alter their appearance [5]. The most common type is that of fillers. These materials are most frequently used to reduce the cost of the material and the dependency of the system on the petrochemical industry. In addition, these materials allow for the alteration of the mechanical properties of the base polymer (matrix) with increases in stiffness typical, while their effect on ultimate strength is dependent on their surface chemistry and, thereby, their interactions with the matrix, among others. The addition of these materials may have a myriad of other effects, ranging from changes in appearance to the modification of the magnetic or electrical properties of the material [6]. Specifically, calcium carbonate (CC) is the most common filler utilised in polymeric systems. It is readily available in a wide range of grades, particle-size distributions and may be compatibilised (frequently through the use of fatty acids or the grafting of polar organic compounds onto the polymer backbone) for improved interfacial interactions with the matrix and reduced sensitivity to moisture [6]. These factors affect its specific behaviour, with smaller particle sizes and compatibilising surface treatments typically resulting in increased mechanical properties, at the cost of toughness [7, 8], for example.

It is notable, however, that HDPE is rarely studied with high loadings of fillers, with the highest loading of CC encountered in literature being 30 vol% (54 wt%) in a rheometric study investigating interparticle and particle-matrix interactions [9]. Indeed, many authors only investigate 30 wt% or less [4, 10, 11, 12, 13]. On the contrary, high loadings (50 wt%) have shown excellent performance in creep tests [14] – with an approximate 60 % reduction in creep at high and low applied loads – and UV stabilisation [15].

Rarer still are studies investigating the interactions between high loadings of fillers and other common additives such as pigments and stabilisers. Pigments, such as carbon black (CB), may serve a myriad of purposes – from the obvious visual alteration to increasing the light stability, stiffness or hardness of the material [16, 17, 18]. Stabilisers, in turn, serve to improve the processing stability of the material, while frequently aiding its light stability – given the identical degradation mechanisms. As in any system, it is common for these additives to interact with one another and the matrix, frequently in surprising ways, with varying impacts on the different properties of the final materials [8]. Some of these combinations have been well studied in the literature, particularly that of CB with various stabilisers. These studies have elucidated, among others, the effects of the additives and their combinations on the thermal stability of the systems [19] and the adsorption mechanics underlying much of the interaction between CB and stabilisers [20, 21, 22, 23].

The processing stability of highly filled materials is a traditional concern, given their increased viscosity [24] and the introduction of compounds that may interfere in the oxidative degradation of the materials, sometimes in unexpected

ways. CC, especially of the coated variety, has been found to have minimal detrimental (sometimes even positive) effects on the thermal stability of materials with which it is compounded at lower loadings. In the case of polyethylenes (PEs), this is due to the function of the calcium stearates that result from the coating process acting as acid scavengers and catalyst neutralisers [8].

HDPE falls victim to the typical autoxidation cycle, with energy (thermal or ultraviolet electromagnetic radiation, typically) driven initiation, followed by propagation and termination steps. This is covered in great detail in established literature, also paying attention to the ways in which primary and secondary antioxidants [2, 8, 25] and hindered amine light stabilisers (HALS) [26] interfere in the propagation steps. Notable, though, is that in PE, particularly HDPE, crosslinking and long-chain branching (LCB) are the dominant degradation mechanism, at least in the early stages [24, 25].

Frequently, the stability of a polyolefin is characterised using a standardised oxidative induction time (OIT) test, performed in a differential scanning calorimeter (DSC) [27]. Here, the sample is heated to a set temperature under an inert atmosphere. Once the material has stabilised at temperature, the atmosphere is switched to an oxidising one and the time until exothermic degradation occurs is monitored. While this serves as a straightforward indication of the oxidative stability of the material, the environment acting to degrade the material is a far cry from what would be encountered in typical melt-processing equipment. Unexpected results may also occur. For example, Irgafos 168 (a secondary stabiliser) may result in reduced OIT results compared to those of a virgin system [19]. Similar drawbacks exist for related methods of characterisation, such as thermogravimetric analysis and the various derivatives of OIT.

While it cannot equal the mechanical stress placed upon a polymer during processing, an alternative is the adoption of a technique typically reserved for the study of viscoelastic properties and gelation in thermosets [28, 29] – time-sweep rheometry. This technique has been applied to the study of polymer degradation, albeit quite rarely. When it is applied in the study of this phenomenon, it is performed under air or nitrogen, typically using oscillatory rheometry at a temperature well above the melting point of the polymer [30, 31, 32]. Dordinejad et al. [30] found that there was no change in the storage modulus of HDPE under a nitrogen atmosphere during an oscillatory test, with the tests at up to 220 °C. The same tests under air, however, produced repeatable, significant increases in storage modulus (G'). Steady-shear measurements are also used, but much less frequently. This is likely due to the reduced amount of data generated, although high-rate tests would appear to proceed much more quickly [33].

In the studies where oscillatory rheometry was used, degradation was frequently assessed through a comparison of the data generated, with no specific measures introduced for more specific comparison [30, 34]. Typically, the G' of the material is the most sensitive indicator, with similar information available through the study of the loss factor (loss modulus (G") divided by G'). The loss factor is frequently expressed as $\tan\delta$, or simply δ – where a 45° angle is indicative of modulus crossover [35]. Studies by Mariani et al. [36, 37] made

use of the time derivatives of the complex viscosities of their HDPE systems to compare the stability of the materials. In their 2002 paper [37], lines tangent to these derivative curves were used to determine "induction times". Here, the "induction time" was the time to the first increase.

The gel point of a system, frequently used in the study of thermosets and typically taken as the point at which the storage and loss moduli of the system are equal (modulus crossover) at a set frequency [28] has also been applied to the study of thermoplastic polymer degradation [38]. It is interesting to note that the time to modulus crossover was found in early works to vary quite linearly with frequency in the medium-to-high frequency range (1 rad/s to 100 rad/s) on a lin-log plot, with levelling-off at lower frequencies (0.1 rad/s to 1 rad/s) [28]. This is due to the stronger impact of local behaviour at the higher frequencies, while macroscopic effects dominate as frequency approaches 0 Hz [39].

A related technique is that of time-resolved mechanical spectroscopy, where a sample is exposed to a cyclical variation in frequency as it "mutates" (through the passage of time, change in temperature, chemical reaction, etc.). This allows for the timely capture of a range of time-series data sets, each at a distinct frequency, allowing the study of the frequency response of a material in the vicinity of any one state [40]. While this technique has been used in the characterisation of polymer degradation [35, 38, 41, 42, 43], such use may have some drawbacks. Chief among these is the complexity of the measurement and the generated data. For this method to work correctly, the material must be held at any one frequency long enough to achieve steady state before the response at that frequency may be recorded. For example, the data given by Salehiyan et al. [41] exemplifies the failure to achieve steady state, particularly in the transition from high frequency to low. This may be seen by their measured storage modulus of the material at 0.1 rad/s exceeding that measured at 0.3 rad/s and 1 rad/s for much of the measured time. Measurement at very low frequencies is complicated by the amount of time required for (even quasi-) steady state to be achieved and the measuring time itself. In turn, this results in excessively long individual frequency sweeps – resulting in reduced time resolution of the final data. For example, Kruse and Wagner [35] were only able to complete a full frequency sweep every $\sim$12.5 min, albeit for a very wide range of frequencies. Their study, too, showed some signs of insufficient stabilisation before measurements were taken – interestingly in the case of a stepwise decline in frequency. In terms of the generated data, isochronous data is not collected, and must thus be inferred through interpolation and/or fitting. Generally, this is useful – for example in the study of ultra-unstable materials, where the zero-time response may be determined through extrapolation [42, 43] – but it is subject to the accuracy of the underlying data.

Based on the above, it is clear that insufficient information exists on the performance of HDPE composites highly filled with CC, particularly in terms of the interactions between various additives in these systems. Further, it is noted – from literature and experiment – that current characterisation techniques and measures do not necessarily yield results suitable for the comparative study of the effects of certain additives on the thermal stability of the materials, partic-

ularly in the presence of Irgafos 168 and/or widely varying loadings of fillers.

These concerns are aimed to be addressed in this paper, through the characterisation of 18 formulations of a HDPE/CC/CB/stabiliser composite system using measures based on the results of OIT- and time-sweep-oscillatory-rheometry-based techniques. For comparison, an unprocessed, unmodified HDPE was also be characterised. To determine the locality and types of degradation, samples taken from the centre, circumference and skin of the materials aged using time-sweep rheometry were compared to unaged samples using Fourier-transform infrared spectroscopy (FTIR). In the process of the study, some differences were found in the measures based on the results generated by the OIT tests and those by the rheometric technique. In the development of this technique, a novel measure for the analysis of degradation was introduced to address an underlying drawback of the rheometric study of gelation. It must be noted, here, that "technique" is used to refer to the technique whereby data were gathered, while "measure" refers to the specific method of analysis of said data.

2. Experimental

2.1. Materials

A commercial injection-moulding grade of HDPE (Dow HDPE 25055E) was used for this study. This was combined with a natural, ultra-fine surface-coated CC (Omya Hydrocarb 95 T – OG), a masterbatched CB (Caparol NEFA MB F 21504 Schwarz – consisting of 28 % Orion Engineered Carbons Printex F 80 in a styrene-ethylene/butylene-styrene (SEBS) copolymer) and a stabiliser pack consisting of BASF Chimassorb 944 and BASF Irgafos 168. Henceforth, these will be referred to as CC, CB and SP (C944 and I168, if discussed separately). To reduce the number of variables, C944 and I168 were held at a constant ratio to one another (3:2), with only the total quantity varied.

Processing was performed on a KraussMaffei Berstorff ZE 25-Cl using an appropriately configured screw (1200 mm, 48 D) with two side feeds. The CB, polymer and stabilisers were introduced in the main feed, with CC introduced through one or both of the side feeds. The melt-temperature profile consisted of a ramp from 220 °C to 235 °C at the die. From here, the material was pelletised. To minimise interference with the degradation states of the materials, these granules were used in the various characterisations.

The formulations were determined through an I- and D-optimal experimental design, based on a quadratic Scheffé-polynomial model. The formulations are given in Table 1. A duplicate centroid was included (10 and 11), as was a duplicate set where two different feed-points for calcium carbonate were investigated for one formulation (01 and 02) outside of the optimal design parameters. This allows the model validity and system behaviour outside of the optimal experimental space to be verified. An unprocessed, unmodified sample of Dow HDPE 25055E was included as reference. The slack-variable [44] representation of the system is given in Figure 1, with HDPE taken as the slack variable.

Table 1: Experimental design – formulations and feed points

	Component (%)					CC feed	
Formulation	HDPE	CC	CB	C944	I168	1	2
Raw	100	0	0	0	0		
01	65.90	30	3.60	0.30	0.20		•
02	65.90	30	3.60	0.30	0.20	•	
03	99.50	0	0	0.30	0.20		
04	100.00	0	0	0	0		
05	97.95	0	1.80	0.15	0.10		
06	95.90	0	3.60	0.30	0.20		
07	96.40	0	3.60	0	0		
08	69.75	30	0	0.15	0.10		•
09	67.70	30	1.80	0.30	0.20		•
10	67.95	30	1.80	0.15	0.10		•
11	67.95	30	1.80	0.15	0.10		•
12	68.20	30	1.80	0	0		•
13	66.15	30	3.60	0.15	0.10		•
14	39.50	60	0.00	0.30	0.20	•	•
15	40.00	60	0	0	0	•	•
16	37.95	60	1.80	0.15	0.10	•	•
17	35.90	60	3.60	0.30	0.20	•	•
18	36.40	60	3.60	0.00	0.00	•	•

2.2. Characterisation

2.2.1. OIT

OIT tests were performed in a way similar to that prescribed in ASTM D3895 – 19 [45], in a PerkinElmer DSC 4000, making use of open aluminium pans. The furnace was heated to 200 °C at a rate of 20 °C/min while under 50 ml/min nitrogen flow. Once at set-point, the material was allowed to stabilise for 5 min, after which the purge gas was changed to air at 50 ml/min. This differs from the typical oxygen purge, as a way of obtaining direct comparability to the test conditions at which time-sweep rheometry was performed. Further, it was found that the onset of degradation occurred too rapidly for ready comparison under oxygen in many samples, but that the oxidation itself was frequently quite gradual. This was resolved through the switch to air. Upon the completion of the test, tangent lines were programmatically fitted according to the method suggested in the standard. Random duplication was implemented, until a satisfactory number of duplicates resulted and at least one formulation was tested in triplicate. This was the case in all characterisation techniques.

To allow comparison, the OIT tests were performed using granules and fine powders. This serves to indicate the effect of viscosity/surface area, as the granules of the highly filled formulations stayed in granular form rather than pooling upon melting. The granules were powdered after cooling in liquid nitrogen (until the nitrogen stopped boiling vigorously) by grinding in a blade grinder until

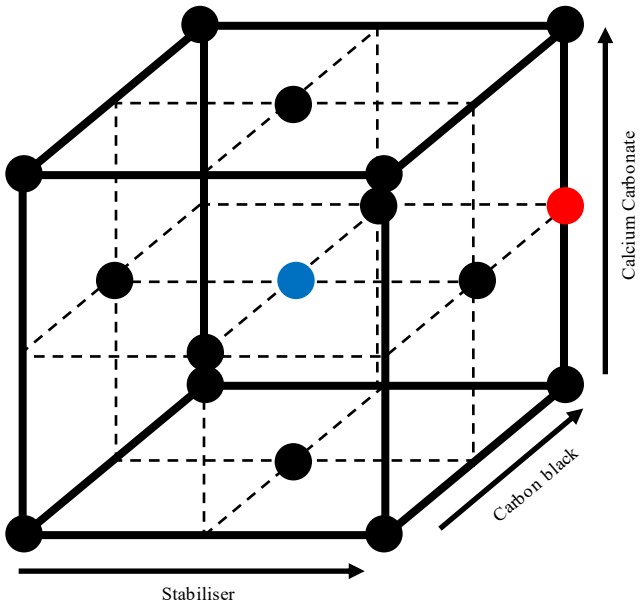

Figure 1: Slack-variable representation of experimental design. The blue dot is the duplicate centroid, while the red dot is the feed-varied duplicate set.[Single column, colour]

a sufficient quantity of composite dust was formed. Any larges particles were removed.

2.2.2. Time-sweep rheometry

The characterisations using time-sweep rheometry were performed on an Anton Paar Physica MCR 301 with a Peltier hood. Tests were performed using 50-mm-diameter parallel plates with a 1 mm gap. Oscillatory strain was set to 1.5 %, to ensure that operation occurred in the linear viscoelastic region. The tests were performed at 200 °C under air. The plates were pre-heated to the set temperature, after which they were separated and the polymer loaded onto the staging area. A slight excess of polymer was used. At this point, the Peltier was closed. Upon melting (2 min after the material was introduced), the plates were brought together and the rim completely trimmed. This was left to equilibrate for a further 3 min, with repeated trimmings of the rim, at which point the test was started.

A range of oscillation frequencies were trialled, from 0.01 Hz to 100 Hz. Further, strain sweeps were completed at the trial frequencies to verify the range of the linear viscoelastic region. At this point, it was decided to make use of a frequency of $10^{-1.5}$ Hz (∼0.031 623 Hz) for the comparative characterisation. The tests were allowed to continue until the torque limit of the machine was reached or δ fell below 10°, whichever came first.

2.2.3. FTIR

Samples were taken from the centre, circumference and skin of the specimens after their time-sweep rheometry tests for comparison to undegraded samples (in the form of granules). Here, circumference denotes the area 3 mm inside the extreme circumference (skin). The samples were taken as soon after the completion of the test as possible. These were characterised using a PerkinElmer Spectrum 100 with the universal attenuated-total-reflectance (UATR) accessory, using a diamond/ZnSe crystal and an accumulation of 16 scans. Care was taken to ensure that the material was flush with the crystal, and covered it in its entirety. The data generated were zeroed on the lowest regions in the vicinity of the carbonyl peak ($\sim$1714 cm^{-1}), with the reference peak ($\sim$730 cm^{-1}) determined through a search for that with minimum variance between the undegraded samples. Based on this data, the carbonyl indexes were calculated for comparison.

2.3. Fitting

Models taking the form of quadratic Scheffé polynomials (Equation 1) [44] were fitted to the generated data using least-squares regression to determine trends and allow more straightforward interpretation of the data. These models were fit to two data sets: a cross-validation data set – omitting Formulation 1 and Formulation 2 to check for overfitting effects – and the full data set. The models for each type of characterisation were compared using their normalised mean absolute errors (nMAE, Equation 2) and their adjusted R^2 (Equation 5) values [44] as most readers will be familiar with these and they provide sufficient information on the quality-of-fit of the models.

$$\hat{y} = \sum_{i=1}^{p} \beta_i x_i + \sum_{i=1}^{p} \sum_{j>i}^{p} \beta_{ij} x_{ij} \tag{1}$$

$$\mathrm{nMAE} = \left(\frac{\sum_{i=1}^{n} |y_i - \hat{y}_i|}{n} \right) \left(\frac{1}{\max y - \min y} \right) \tag{2}$$

$$\mathrm{SSE} = \sum_{i=1}^{n} (y_i - \hat{y}_i)^2 \tag{3}$$

$$\mathrm{SST} = \sum_{i=1}^{n} (y_i - \bar{y})^2 \tag{4}$$

$$\mathrm{adj.R}^2 = 1 - \frac{\mathrm{SSE}(n-1)}{\mathrm{SST}(n-p)} \tag{5}$$

Where $\hat{y}_i$ is the predicted value for y_i, $\bar{y}$ is the mean of y, β is a constant, n is the number of observations, p is the number of mixture components, SSE is the standard squared error and SST is the total squared error.

3. Results and discussion

3.1. OIT

3.1.1. Granules

Starting with the most common and straightforward of the stability tests – OIT using granules – it is useful to first investigate an overview of the data generated and the predictions of the models fitted (Figure 2). The fitted parameters are provided in the supplementary information, Table S1, along with those for all of the other models. Linear and special-cubic Scheffé polynomials were also fitted to the data in all cases, but were found to provide markedly inferior fits in the prior case (with a maximum adjusted R^2 of 0.737 in the linear case) or the potential for severe overfitting in the latter case (as verified by the prediction of extreme values during cross-validation). From this, it is clear that the additives have a significant and complex impact. Regarding OIT making use of granules, the quadratic models allow far better fits. Nonetheless, perfect fits are not achieved. Most notable is the weakness of fit in cases with the maximum loading of SP, with over predictions in the case of Formulation 1, Formulation 2 and Formulation 3 and an under prediction in the case of Formulation 17 (with the maximum loadings of all additives). The latter is particularly interesting, considering that the very similar Formulation 16 is overestimated. Coupled with the cross-validation results – where one may find that overfitting does not appear to be the case, there is a strong case for unmodeled underlying complexity (albeit weak). Based on this and a comparison of the quality-of-fit metrics, the quadratic model fitted to the full data set (adjusted R^2 of 0.918, nMAE of 0.0395) is taken as the most valid.

Of further interest is the comparison of the data generated for Formulation 3 and Formulation 4. Here, the OIT of Formulation 3 is very similar to that of Formulation 4, despite Formulation 3 having the maximum SP loading while Formulation 4 is unstabilised. If, however, one further studies the underlying data, it is notable that the most exothermic point in the oxidation of Formulation 3 occurs much later than that of Formulation 4. This may be seen in Figure 3, where the times to minimum value (most exothermic points in the degradations, henceforth TMV) for all of the formulations are compared. This suggests that, while the onsets are similar, Formulation 3 is more stabilised than Formulation 4. This would indicate a weakness in the standard way of analysing data of this sort. The other results based on TMV differ quite significantly from those based on the standard method. Particularly, the highly stabilised materials containing CB at the 0 % and 30 % CC loadings (Formulation 6, Formulation 9) now perform dramatically better in comparison to the other materials, even surpassing Formulation 17 (which was the most stable in the prior measure). Also notable is the performance of Formulation 14 – more closely matching that of Formulation 17. There is, however, substantial variance between samples of the same formulation (Formulation 3, Formulation 5, Formulation 8, Formulations 10/11 and Formulation 16). This does not appear to be much more severe than was the case with the standard method, indicating that the cause is non-ideal mixing of the materials and/or an inherent issue with

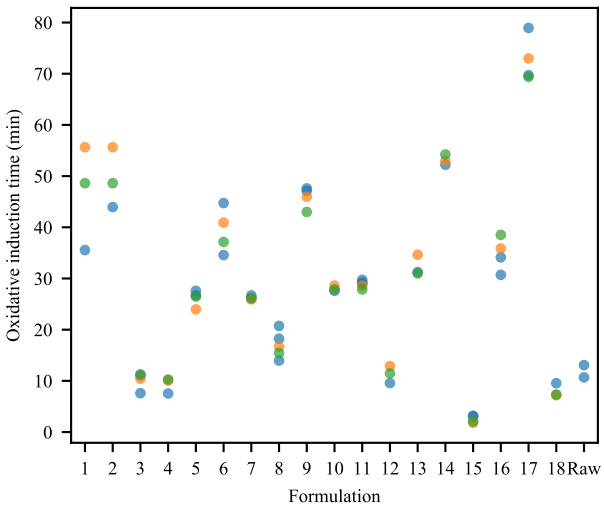

Figure 2: Granular OIT experimental results (●) with model predictions for the full (●) and cross-validation (●) models. [single column, colour]

the technique. In terms of the fitted models, the model fitted to the full data set (adjusted R^2 of 0.853, nMAE of 0.0724) was found to offer the best match to the experimental data.

Finally, the predicted results (Figure 4) may be investigated to gain a better idea of the inherent trends of the system. From this figure, it is clear that, broadly, higher loadings of the additives serve to increase the OIT of the system. In terms of the pure-component effects (therefore in systems only containing HDPE and the noted additive), CB increases the OIT of the system while CC reduces it – although with diminishing returns in either case. In agreement with the earlier results, SP has little effect. There exists an interesting contrast to this in the predictions for the TMV model (Figure 5). There, SP plays the role expected of it, with strong positive pure-component effects that are nearly linear in nature. The negative pure-component effect of CC is reversed to the point of it having a weakly positive effect, while CB maintains its positive primary effect.

This changes dramatically when considering interactive effects (Figure 6), most notably through the dependency of SP effectivity on the CC lo§ading, with high loadings of CC greatly improving the effect of SP addition. A similar, albeit much weaker effect exists between CB and SP. Conversely, the CC/CB interaction is weakly antagonistic.. These figures are used to isolate (and better study) the interactions between sets of additives, based on the definitions provided by Brydson [2]. Figures of this type are created by removing the binary effects between the varied additives and those held constant – thereby isolating

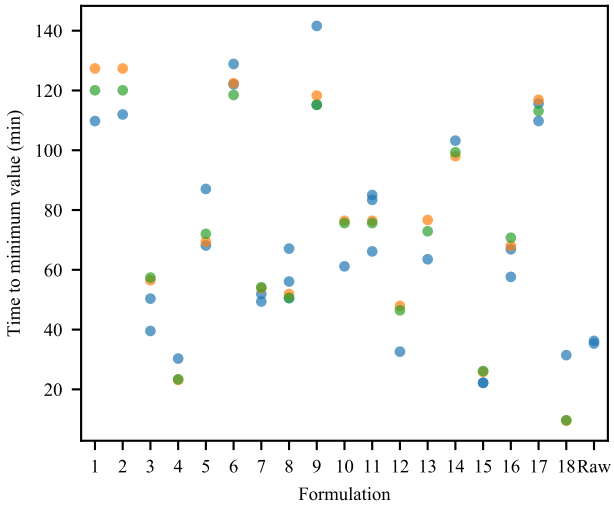

Figure 3: Granular TMV experimental results (●) with model predictions for the full (●) and cross-validation (●) models. [single column, colour]

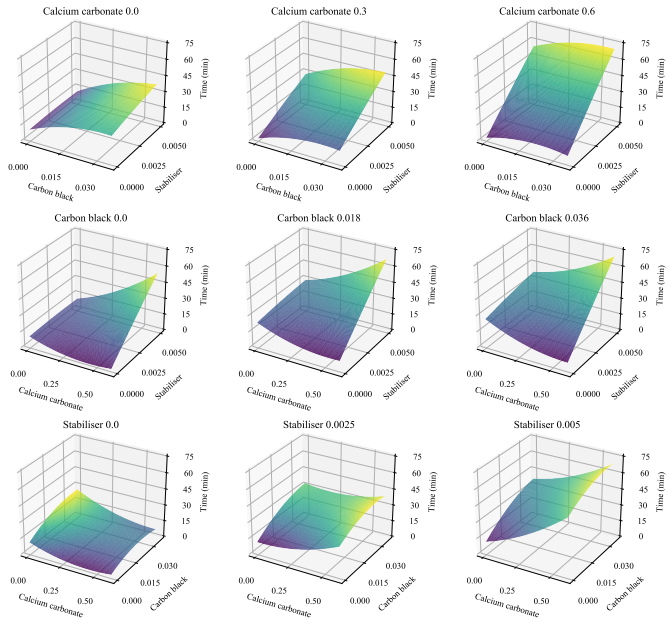

Figure 4: Granular OIT model predictions. [2-column, colour]

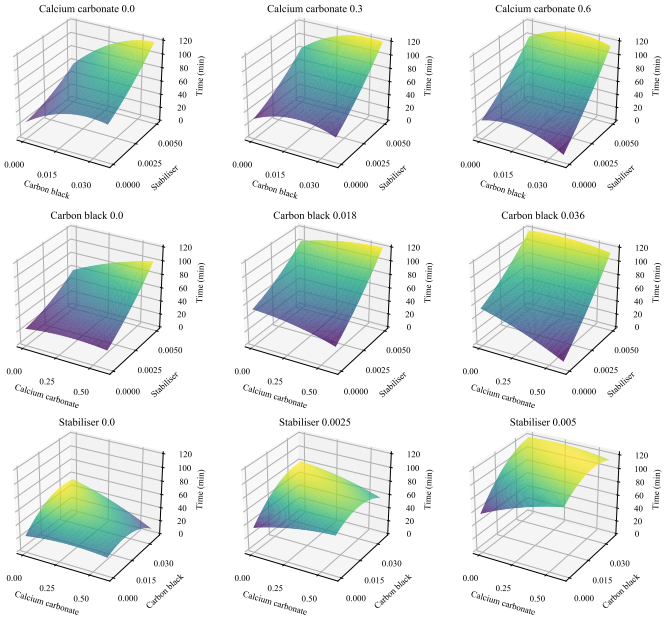

Figure 5: Granular TMV model predictions. [2-column, colour]

the interactions between the varied additives. This is particularly necessary as the fitted constants in Scheffé polynomials are not suitable for intuitive analysis. In these figures, the transparent red plane is indicative of purely additive effects, with results above it indicative of synergism, while those below it are indicative of antagonism. Figure 7 mirrors the results suggested by Figure 6, although the strengths of the interactions are much more balanced – with the strongest interaction now the CB/CC antagonism.

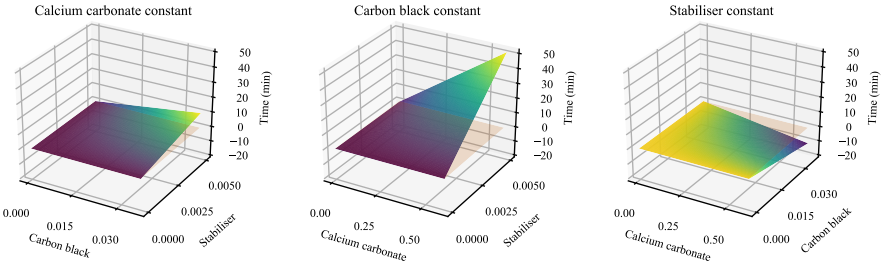

Figure 6: Granular OIT model interactions. [2-column, colour]

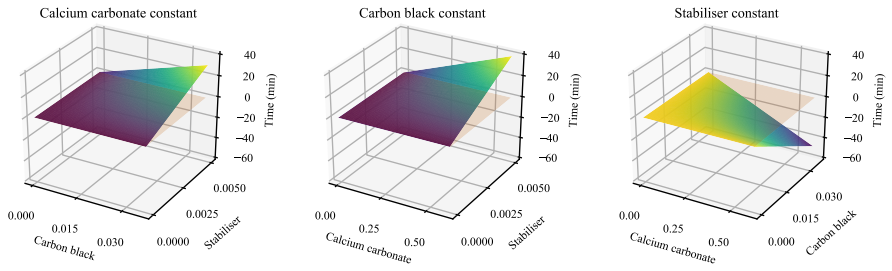

Figure 7: Granular TMV model predictions. [2-column, colour]

3.1.2. Powders

The strange behaviour of Formulation 3 compared to Formulation 4 in the OIT measure is worsened in the case of the powdered samples, with even earlier onset (Figure 8 and Figure 9). This is likely to stem from the increased exposed surface area – visible through the reduced OIT and TMV values. Otherwise, notable is the large variance for individual formulations and between identical formulations, particularly Formulation 1, Formulation 2 and Formulation 10/11. This is also visible through the quality-of-fit metrics, with the best models – fitted on the complete data set – having adjusted R^2 values of 0.853 (OIT) and 0.846 (TMV) and nMAEs of 0.0611 and 0.0814. The data for TMV is interesting, in that it is very balanced, with fairly clear distinctions between the different stabiliser levels in the formulations. Despite this, however, there are numerous cases of strong under-/over-prediction by the models, giving credence to the theory of significant unfitted effects.

The model results are very similar to those of the granular samples in the case of OIT (Figure S1 in supplementary information), albeit with a negative primary effect for SP and a predicted turning point in the negative effect of CC. The primary-effect TMV results (Figure S2 in supplementary information) are also very similar to those of the granular samples, with only slightly different curvature. An investigation of the secondary effects (Figure S3 and Figure S4 in supplementary information) also reveals interesting deviations from the granular results, with virtually purely additive effects between CB and SP and CB and CC in the OIT model. At the same time, the TMV model suggests stronger synergism between CC and SP and somewhat weaker antagonism between CB and CC than seen in the granular case. CB and SP are limited to additive effects in this case too.

3.2. Time-sweep rheometry

In the pursuit of a method suitable for the comparison of materials with very different filler loadings – owing to the impact of fillers at higher loadings on the point of modulus crossover (Figure 10, along with the predictions of fitted models) – a novel technique was developed. In this technique, the storage modulus is plotted to time, on a log-log axis. When this is done using the materials of this study, a series of distinct steps may be seen (Figure 11, lines

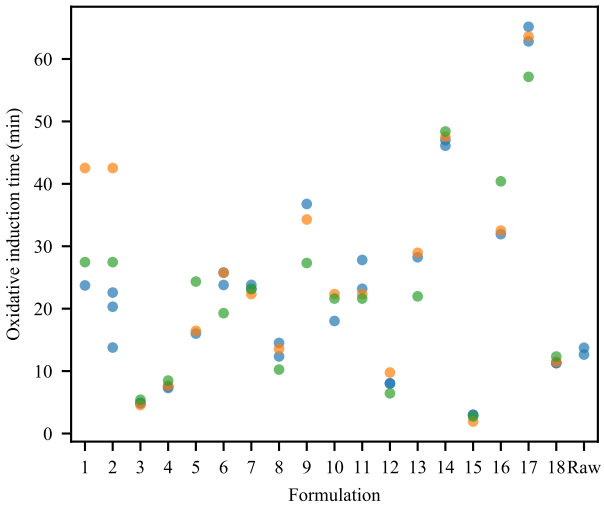

Figure 8: Powder OIT experimental results (●) with model predictions for the full (●) and cross-validation (●) models. [single column, colour]

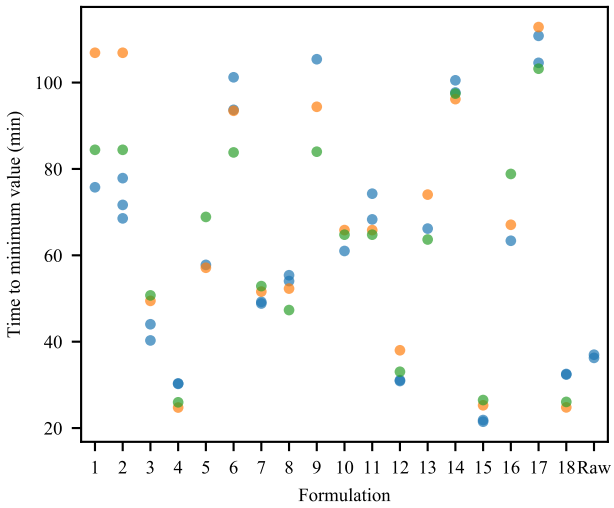

Figure 9: Powder TMV experimental results (●) with model predictions for the full (●) and cross-validation (●) models. [single column, colour]

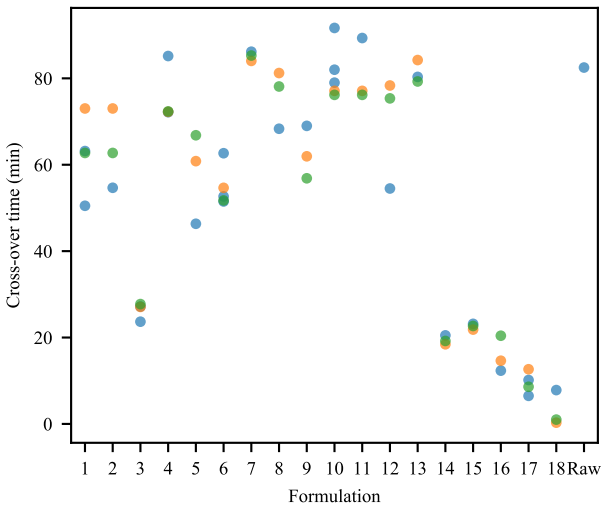

Figure 10: Rheometric time-sweep modulus cross-over experimental data (●) with model predictions for the full (●) and cross-validation (●) models. [single column, colour]

and intersection discussed in the next paragraph). First – in the more stable materials – dead-time (the length of which is also a function of the oxidative stability of the material, albeit with a stronger dependence on CB and CC). Thereafter, a turn upward, with a linear rise. This levels off to some extent for some time, after which another turn upward occurs. This also contains linear elements (on the log-log plot), but these may take some time to materialise. Eventually, this, too, levels off. The systems containing CC at a 30 % loading and CB exhibited double-plateau behaviour (Figure 12). This was also found in Formulation 15, but none of the other formulations that contained 60 % CC exhibited such behaviour.

If these changes – particularly the final upward turn – are investigated, they may be seen to offer correlation with the oxidative stability of the material with minimal dependency on the filler loading. To repeatably determine the time at which this turn occurs, inspiration was taken from OIT tests. In doing so, straight lines are fit to the pseudo-linear sections on the log-log plot (Equation 6 and Equation 7) and their intersection noted (Figure 11 and Figure 12). The time at which the intersection occurs is taken as the time-measure of the turn. This is henceforth referred to as the degradation onset time (DOT). The data generated using this technique may be seen in Figure 13 for comparison to that in Figure 10. This, clearly, far better represents the stability of the system than the point of modulus crossover, also referencing Figure 2, Figure 3, Figure 8 and Figure 9. The fact that Formulation 6 performs best in this measure serves as confirmation of this, as it is expected to be the most stable formulation –

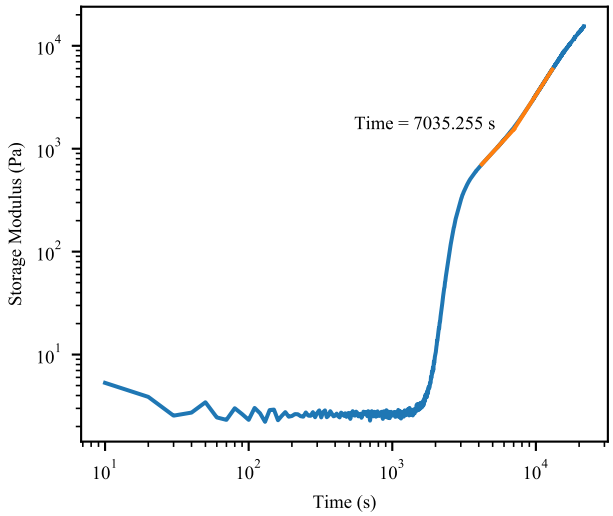

Figure 11: Time-dependent storage modulus of Formulation 5 (——) with tangent lines (——) and degradation onset time. [single column, colour]

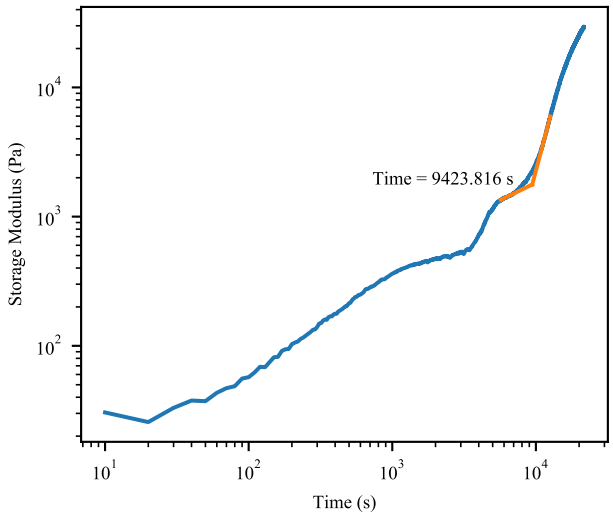

Figure 12: Time-dependent storage modulus of Formulation 9 (——) with tangent lines (——) and degradation onset time. [single column, colour]

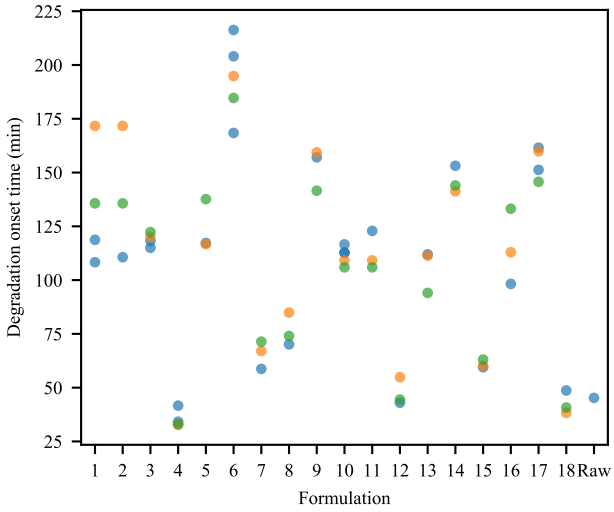

Figure 13: Rheometric time-sweep DOT experimental data (●) with model predictions for the full (●) and cross-validation (●) models. [single column, colour]

through maximum loadings for SP and CB and no CC.

$$\log_{10} G' = m \log_{10} t + c \tag{6}$$

$$G' = t^m \cdot 10^c \tag{7}$$

Where t is the time since the start of the run, m is the slope of the line on the log-log plot and c is the intercept on the log-log plot.

The reason for the reduced time to modulus crossover in materials with higher filler loadings is clear through the investigation of the initial δ data (Figure 14). These data were taken after 100 s to allow the samples to stabilise at the oscillation frequency. The storage moduli of the highly filled materials are increased, likely through particle effects [14], thereby decreasing the loss factors.

While some of the quality-of-fit metrics of the fitted models (quadratic, full set) are not exceptional, with adjusted R^2 values of 0.817 (DOT) and 0.824 (modulus crossover), the nMAEs of 0.0735 and 0.0783 are more acceptable. When this is coupled with the broad dispersion of results throughout the measurement area, high confidence in the predictions may be had.

The DOT model (Figure 15) shows the initially negative primary effect of CC, eventually turning to a positive primary effect at a ∼45 % loading. Further, the strong and very strong positive primary effects of CB and SP may also be seen. It is interesting to note that this is the one case where the most

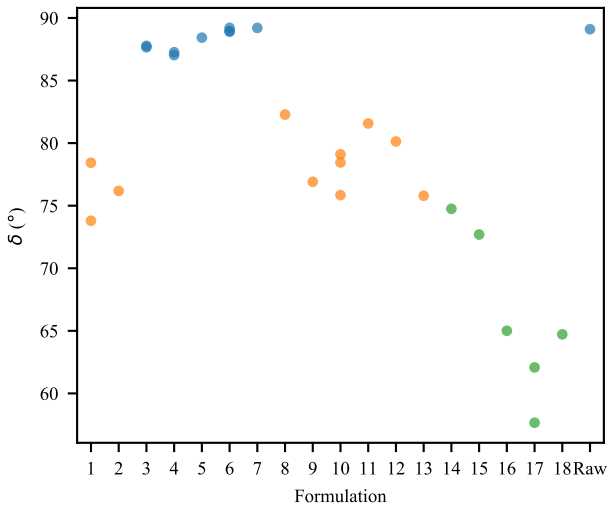

Figure 14: Initial δ values for the different calcium carbonate loadings (0 % (●), 30 % (●) and 60 % (●)) of the formulations. [single column, colour]

stable combination is not that of maximum CB, CC and SP loadings (Formulation 17), but rather maximum CB and SP loadings, coupled with no CC (as shown experimentally with Formulation 6).

The secondary interactions of this model may again be studied on their own (Figure 16). Here, the strong antagonism between CB and CC is again clear, but there are no strong synergisms to counteract its effect. The very weak antagonism between CC and SP is a major departure from the behaviour of the system in the OIT studies, while the CB/SP interaction is among the strongest of its estimations in the prior measures.

The model of the modulus-crossover time (Figure 17) very clearly tells a story of negative primary effect of CC at high loadings, despite its positive primary effect at lower loadings. Indeed, said negative primary effect dwarfs all of the other effects, even combined. Adding further doubt to the utility of a measure of this sort to the determination of the thermal stabilities of a range of materials is the fairly strong negative primary effect of SP. This is offset by a nearly linear positive primary effect in the case of CB.

Making a return to the secondary interactions (Figure 18) is the CC/SP synergism. Conversely, the ever-present CB/CC antagonism again makes an appearance, as does the weak CB/SP synergism.

3.3. Oxidative stability

Clearly, based on the results of the OIT and time-sweep tests, the results of one test do not necessarily reflect on another, and must, therefore, be taken

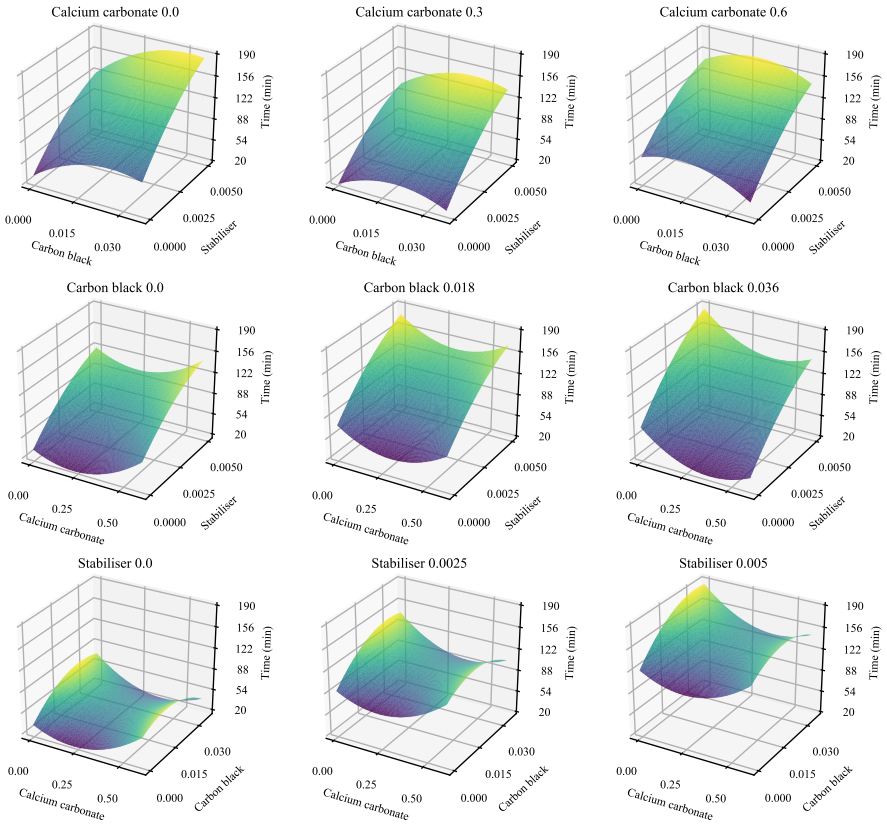

Figure 15: Rheometric DOT model predictions. [2-column, colour]

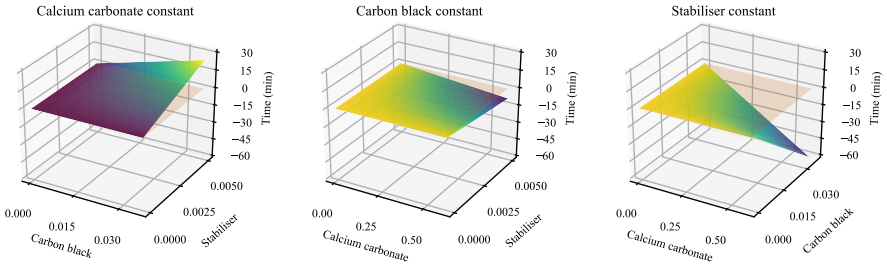

Figure 16: Rheometric DOT model predictions – secondary effects. [2-column, colour]

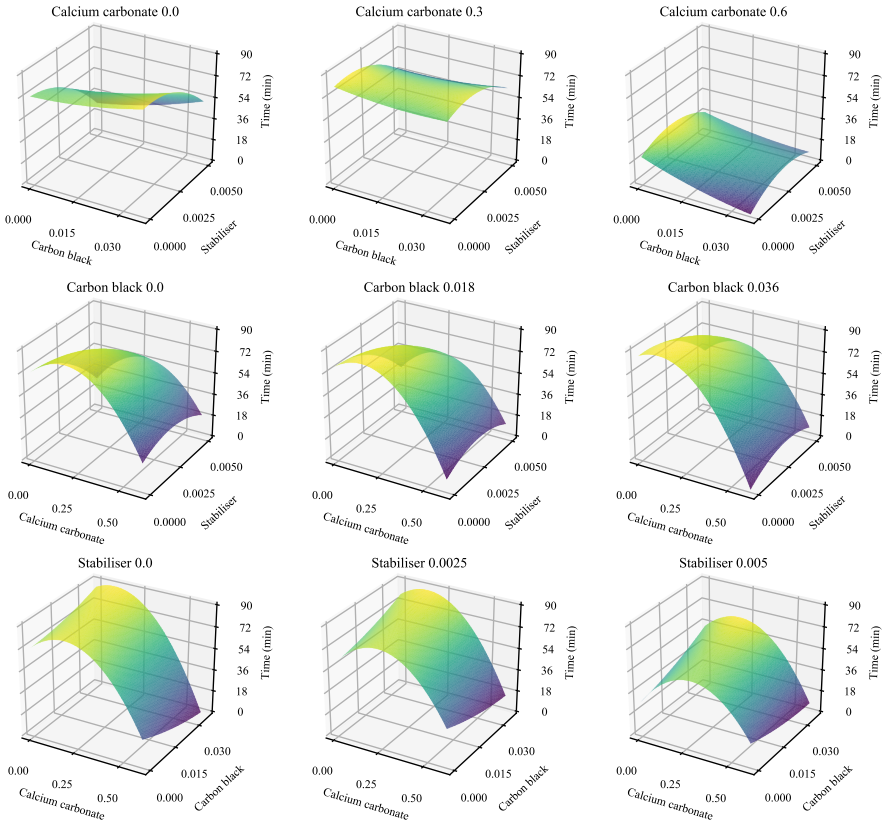

Figure 17: Rheometric modulus cross-over model predictions. [2-column, colour]

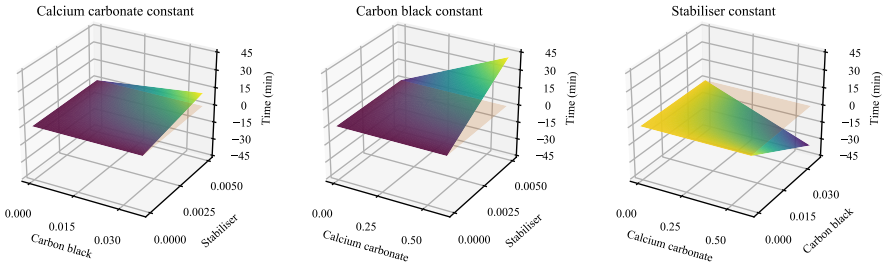

Figure 18: Rheometric modulus cross-over model predictions – secondary effects. [2-column, colour]

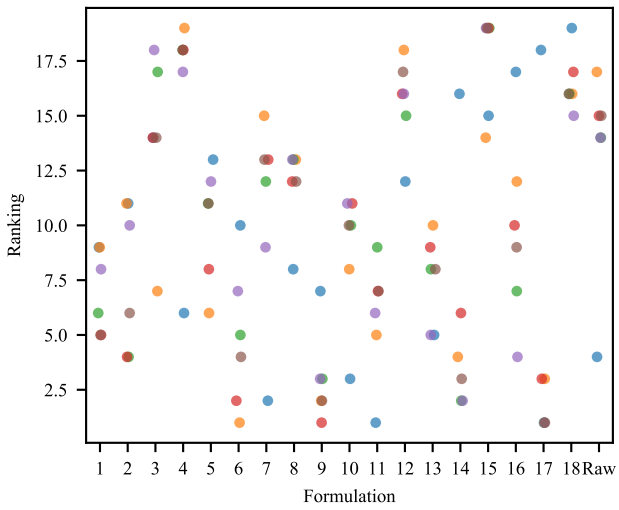

Figure 19: Comparison of the rankings (cross-over time (●), DOT (●), granular OIT (●), granular TMV (●), powder OIT (●) and powder TMV (●)) of the materials in the different tests and measures. [single column, colour]

in context. An investigation of the rankings of the formulations in each material confirms this (Figure 19). If, dropping the modulus cross-over results, the rankings are added, clarity is gained (Figure 20). Four of the most-stabilised materials occupy the top four positions while five of the unstabilised materials occupy the bottom five positions. Not all is so clear, however. Formulation 1 and Formulation 2 under-perform to a degree, given their maximum stabilised loadings and, yet, middling performance. The variance between the rankings of Formulation 10 and Formulation 11 is more indicative on the sensitivity of this method than experimental variance, given the similarity of their results in the tests.

Nonetheless, some general observations may be made through inference from the combination of the various models. The SP, likely with I168 dominating, performs its role well, albeit with curious results in the OIT measurements. In all other measures, however, it performs as expected. Similarly, the CB masterbatch showed positive primary effects in all cases. CC, conversely, exhibited negative primary effects, albeit with strong turning points in some cases. The antagonism between CB and CC is present in all cases, although its strength varies. Similarly, CB and SP exhibit additive effects (in two cases) or, typically, interact synergistically. The extremely strong synergism between CC and SP is present in all but one of the measures, with additive effects in that (DOT).

Literature would suggest mixed interactions between CC and SP, with (ostensibly) un-coated CC having been found to exhibit antagonistic interactions

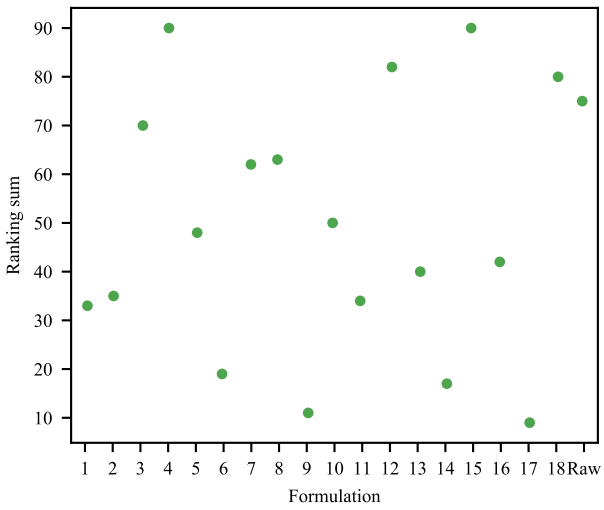

Figure 20: Comparison of the summed rankings of the materials (modulus cross-over omitted). [single column]

with HALS [46, 47], while secondary antioxidants based on phosphite chemistry exhibit synergistic complexing with calcium (in the form of calcium stearate)[48]. The antagonistic interactions between HALS and CC were ascribed to adsorptive effects – instead of complexation – in the mechanistic work by Hu, XU and Zhang [46] in isooctane. Conversely, HALS have been shown to exhibit synergistic effects with calcium stearate in the presence of phenolic antioxidants (which may be found at low loadings in commercial HDPE), through the suppression of the oxidation of the phenol to an active quinone [49]. It must be noted, however, that there exists a substantial body of evidence in the literature that the testing temperatures involved in OIT are too high for the effects of HALS to be seen to a significant extent, despite its tremendous long-term impact on the stability of materials in which it has been used at lower temperatures [18]. Significant interaction of the CC itself (excluding calcium-coating compounds) with C944 or I168 is doubtful, as compatibilised CC has been shown to function optimally with complete surface coverage by the compatibiliser [50]. A more likely explanation is that of synergism between the coating and the SP, with any mobile coating acting as an acid scavenger and catalyst neutraliser [8]. Further, synergisms were found between I168-containing stabiliser packages and calcium stearate, with these ascribed to the above and the formation of phosphite/calcium complexes – resulting in more effective hydroperoxide decomposition and, thereby, the inhibition of carbonyl formation [48]. This may be aided by the effective increase in the concentration of the SP in the polymer, given the displacement of polymer by CC. Another possibility is that of rheological interference. This

is noted due to the lack of pooling in the more highly filled granular materials – with these materials remaining in their granular form throughout the tests – giving rise to variable surface areas for diffusion and reaction. This may give frivolous results at CC loadings higher than ∼30 % in the OIT tests. While this was sought to be remedied by the use of the powdered samples, a lack of fusion between the particles could clearly be seen in the most viscous of the materials (Formulation 14 and Formulation 15).

There also exists historic precedent for synergism between CB and SP, with Peña et al. [19] having found individual and overall synergisms between CB (furnace, two types: clean and high O/S), C944 and I168 in the OIT testing of LDPEs at 200 °C. As mentioned in the introduction, these authors found I168 to have a weakly negative primary effect, while they found CBs had a weakly positive primary effect. C944 was found to have a slightly more positive effect. While it has been found that HALS may be adsorbed by CB, with the strength of this activity based on the surface groups and topography of the CB and the structure and functional groups of the HALS [22], this does not explain the synergy between the compounds – indeed to the contrary. This effect, however, is likely to be somewhat suppressed in this case, as the CB used possesses a basic surface chemistry (with a pH of 9.0). Peña et al. [20, 19] reasoned that a more acidic CB would adsorb HALS more strongly than a less acidic CB, owing to acid-base interactions and hydrogen bonding with carboxylic and phenolic groups, while other groups are limited to hydrogen bonding. This, however, is countered by the less-hindered nature of C944 compared to that of other polymeric HALS and the presence of secondary amines in its side groups, found by Peña et al. [22] to encourage adsorption. Adsorption does not appear to present a problem in the case of I168, as it exhibits minimal adsorption on a basic (with a pH of 7.4) carbon black in medium-density polyethylene and on a variety of CBs in *n*-heptane [51, 21]. This has been suggested to be due to severe steric hindrance – owing to the central location of the phosphite group (which typically promotes adsorption) in the molecule [21].

The improvements brought about by the addition of CB likely stem from a combination of the reduced viscosity of the system – owing to the introduction of SEBS – and the thermally stabilising nature of certain carbon blacks. The latter was ascribed to the presence of oxygen groups on the surface of the CB that serve to decompose hydroperoxides and the radical trap/chain breaking behaviour of the CB [19, 52]. The prior is based on the shear/viscosity-dependency of HDPE degradation. Rideal and Padget [24] found that the rate of LCB in low-vinyl HDPE is increased (by near order-of-magnitude levels) at lower melt temperatures (212 °C compared to up to 306 °C) in a Brabender Plastograph under nitrogen and air. High-vinyl HDPE strongly favoured chain-scission reactions. The carbonyl index was also found to have an inverse proportionality to melt temperature in the low-vinyl polymer. Given the extremely low vinyl content of the base polymer in the present study, it is likely that a decrease in viscosity will result in a substantial reduction in LCB reactions.

This viscosity effect likely explains much of the negative primary effect of CC addition, in addition to the antagonism of CB and CC (as CC addition undoes

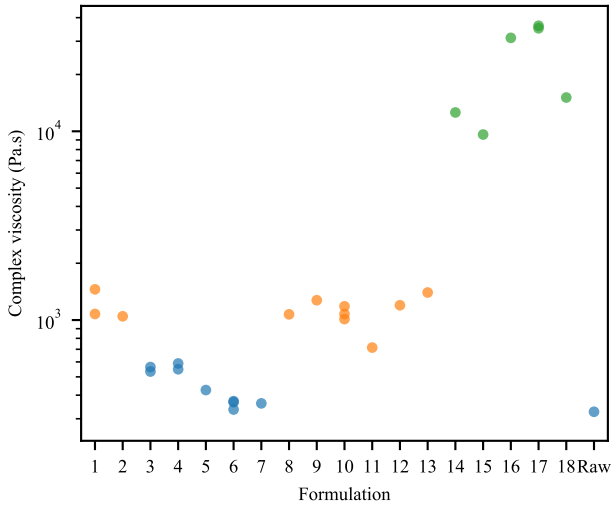

Figure 21: Impact of calcium carbonate loading (0 % (●), 30 % (●) and 60 % (●)) on the initial complex viscosities of the formulations (100 s stabilisation time). [single column, colour]

the reductions in viscosity brought about by the addition of SEBS to the composite (Figure 21)). No records of the antagonism between CB and CC were found in the literature. However, Bai et al. [53] found a negative primary effect on the thermal stability for stearate-coated CC in ABS, potentially indicating some type of antagonistic interaction between CC and butadiene/styrene-containing polymers. Viscosity, however, remains likely to be the dominant effect, as the negative primary effects found by Bai et al. [53] were relatively weak.

There is some precedent in literature for the intermediate plateau seen in Figure 11. It may be found in the 170 °C plot of complex viscosity against time of HDPE by Mariani et al. [36], although undiscussed, and in stabilised samples of LLDPE studied by Dordinejad et al. [30], where it was ascribed to the late-onset antioxidative effect of Irganox 1010, a primary stabiliser. Their system also contained I168, which this did not result in plateau behaviour on its own, although it did modify the behaviour in the presence of the primary stabiliser. Given that all of the formulations studied here exhibited plateauing behaviour, it is likely that a primary stabiliser is included in the DOW HDPE 25055E base polymer.

In terms of the characterisation techniques and measures, it is clear that modulus cross-over is not an ideal measure for systems with widely varying loss factors. In similar terms, it is unlikely that OIT tests provide accurate representations of the performance of systems containing little other than secondary antioxidants. This is reiterated by the comparatively weak performance of Formulation 6 in these tests. The more straightforward granular method does not

yield quantifiably worse results than those of the powder method. On the contrary, in fact, in terms of the prior secondary antioxidant results. Little can separate the remaining three methods in terms of validity, given the current data set. From a practical standpoint, the dramatically longer run-times and added analytical complexity of the DOT method are not desirable. However, its results exhibit less single-formulation variance than those achieved by either TMV method. This is due to the far larger sample requirement (∼2 g compared to <30 mg) of the rheometric methods, which reduces the impact of local variances due to non-ideal mixing – giving a far better indication of average behaviour of the system.

3.4. FTIR

The FTIR spectra collected for the samples all possess the characteristic bands of polyethylenes to some extent. These consist of $-(CH_2)_n-$ rocking (∼700 cm^{-1}), deformation vibration (1445 cm^{-1} to 1485 cm^{-1}) and stretching bands (2840 cm^{-1} to 2950 cm^{-1}) [54, 55]. The addition of CC results in the addition of its characteristic strong band at ∼1420 cm^{-1} to the spectrum [55].

The predominant bands that accompany degradation were found to be those of C=O stretching (1712 cm^{-1}, 1728 cm^{-1} and 1772 cm^{-1}) and C–O or C–O–C stretching (1170 cm^{-1} to 1178 cm^{-1}) [55]. These may be very clearly seen in the extremely degraded samples, such as the skin of Formulation 4 (Figure 22). Here, the skin is a 0.2-mm-thick film formed on the outer edge, with a noticeable difference in texture and appearance with severe yellowing/browning in the materials without CB. In these extreme cases, far weaker bands belonging to C=C bending (910 cm^{-1} to 990 cm^{-1}) [54], C=C stretching (1630 cm^{-1} to 1680 cm^{-1}), further C-O and C-O-C stretching (1030 cm^{-1} to 1270 cm^{-1}) and O-H bending (1260 cm^{-1} to 1440 cm^{-1}) may be seen [55]. In the extreme cases, peak broadening occurs, resulting in not all of the peaks of the less-aged materials being suitable as reference for the carbonyl peaks. Based on this, the upper $-(CH_2)_n-$ stretching band (∼2950 cm^{-1}) is chosen as the reference peak.

The specific C-O bands would suggest the presence of primary (1030 cm^{-1} to 1085 cm^{-1}) and secondary (1075 cm^{-1} to 1125 cm^{-1}) alcohols, saturated aliphatic ethers (1060 cm^{-1} to 1150 cm^{-1}) and/or saturated aliphatic esters (1150 cm^{-1} to 1270 cm^{-1}) . The C=O (carbonyl) bands, meanwhile, may be indicative of many of the typical oxidative degradation products of HDPE, including aldehydes, ketones and carboxylic acids. Of these, aldehydes may be eliminated, as their characteristic band at 2710 cm^{-1} is absent [55, 56].

Through the use of FTIR and localised samples, it is possible to determine to some extent the progression of oxidative degradation through the samples through the use of the carbonyl index (Figure 23).

Based on the dramatically increased carbonyl indexes of the skin samples and the negligible difference between the unaged granules and the central and circumferential areas, it is clear that the skin acted as an oxygen barrier/sink – preventing the conventional oxidative degradation of the internal areas of the test discs. What is notable here, too, is that the outer layer had to be broken before the measuring tool could be retracted, in many cases. This suggests that

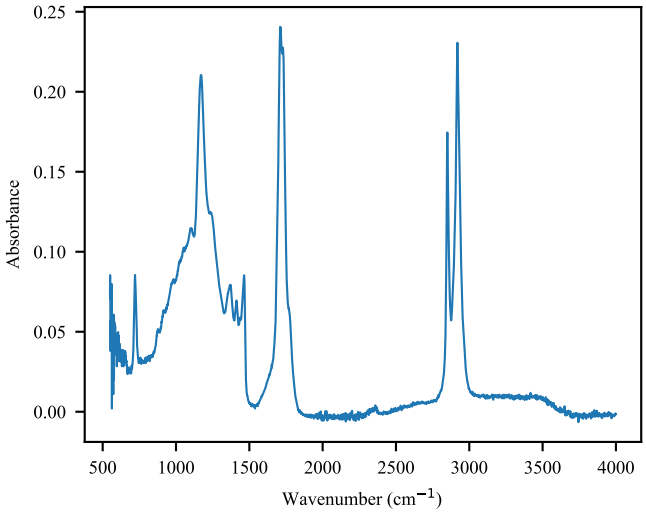

Figure 22: FTIR spectrum of the skin of Formulation 4. [single column]

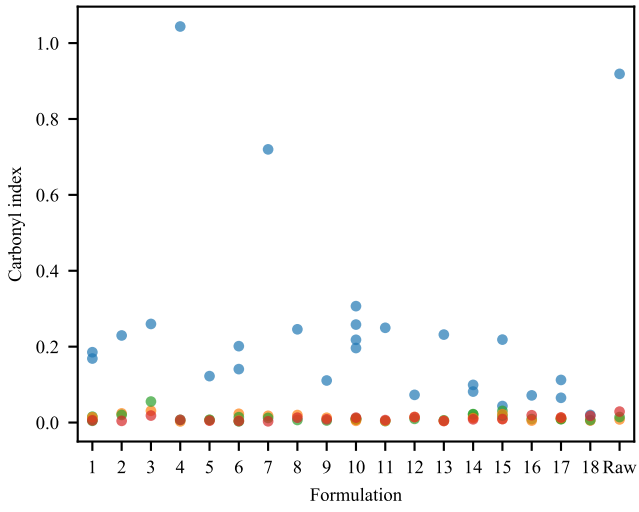

Figure 23: Localised carbonyl indexes (skin (●), circumference (●), centre (●) unaged (●)) throughout the formulations. [single column, colour]

a large part of the cross-linking and LCB was limited to the radial area, even after significant passage of time. This may be confirmed with gel-permeation chromatography [57] on the particulate-free samples, but that is outside the scope of this study.

Nonetheless, it is believed that there is some truth in the model proposed by Filippone et al. [42], with cross-linking working inward – albeit slowly – from the radius. Particularly, the highly-localised area of autoxidative degradation on the skin would likely serve as a primary radical source. The low chain mobility in the system – partially owing to operation in the linear viscoelastic region – then results in a sharp decline in radical activity as one moves inward from the radius. The inner area will be preferentially subject to LCB and crosslinking in the absence of competing reactions with oxygen, albeit with relatively few radicals to initiate the reactions.

4. Conclusion

The primary and secondary effects of a CB, CC and SP on the oxidative stability of a commercial grade of HDPE were determined. The oxidative stability was assessed through OIT- and oscillatory-time-sweep-rheometry-based techniques. The progression of degradation through the time-sweep-rheometry samples was assessed through the use of ATR-FTIR spectroscopy. Through these techniques, it was determined that all of the components had strong primary effects – positive in the cases of the CB and SP, negative in the case of CC. Interactions were also found, with weak synergism between CB and SP, strong synergism between CC and SP and strong antagonism between CB and CC. The causes of these interactions were discussed based on available literature.

The oxidative degradation of the time-sweep-rheometry samples was found to be isolated to the skin area, with severe degradation, while the inner material was virtually unaffected by oxygen. A wide range of the degradation products were identified. LCB and/or cross-linking effects were found to be preferred over chain-scission effects through the studies by time-sweep rheometry. The locality of these effects may be the subject of a further investigation.

The data gathered allowed for the comparison of the techniques and measures used, with the modulus-cross-over measure frequently used in studies of thermosets found to be ill-applicable to the study of materials with a wide range of starting viscosities. OIT techniques were found to yield questionable results in materials containing little other than stabilisers, with the oddity ascribed to effects pertaining to Irgafos 168, confirmed in a prior study. A novel measure of degradation onset was created for use with time-sweep rheometry, which yielded comparable results to those of the most exothermic point in the oxidation of samples in a differential scanning calorimeter.

5. Acknowledgements

The authors acknowledge the Leibniz-Institut für Polymerforschung Dresden e. V. for providing many of the facilities required for this research. The au-

thors would like to thank their colleagues at the University of Pretoria and the Leibniz-Institut für Polymerforschung Dresden e. V., particularly Bianca Gevers, Dr Shatish Ramjee, Dr Ines Kühnert, Dr Andreas Leuteritz and Dr Roland Vogel, for their advice and discussions on this work. Further thanks are due to Omya of Oftringen, Switzerland, and Caparol Industrial Solutions of Grimma-Nerchau, Germany, for the materials that they provided. The authors would also like to thank Techsparks (Pty) Ltd and the Technology and Human Resources for Industry Programme (THRIP) (grant number THRIP/133/31/03/2016), administered by the Department of Trade and Industry, South Africa, for their contribution to a travel allowance for WD Viljoen to visit the Leibniz-Institut für Polymerforschung Dresden e. V. WD Viljoen is also thankful to the Leibniz-Institut für Polymerforschung Dresden e. V. for the stipend he was provided during his stay.

6. Data availability

The raw/processed data required to reproduce these findings cannot be shared at this time as the data also forms part of an ongoing study.

References

[1] C. Dobbin, An industrial chronology of polyethylene, in: A. Chatterjee, M. A. Spalding (Eds.), Handbook of Industrial Polyethylene and Technology, John Wiley & Sons, Inc., New Jersey, 2017, Ch. 1, pp. 3–24.

[2] J. A. Brydson, Plastics materials, Butterworth-Heinemann, Oxford, 1999.

[3] F. Du Toit, R. Sanderson, W. Engelbrecht, J. Wagener, The effect of surface fluorination on the wettability of high density polyethylene, Journal of Fluorine Chemistry 74 (1) (1995) 43–48.

[4] R. Yang, J. Yu, Y. Liu, K. Wang, Effects of inorganic fillers on the natural photo-oxidation of high-density polyethylene, Polymer Degradation and Stability 88 (2) (2005) 333–340.

[5] G. Pritchard, Additives are essential, in: G. Pritchard (Ed.), Plastics Additives, Springer, Berlin, 1998, Ch. 1, pp. 3–10.

[6] G. Wypych, Handbook of Fillers, 4th Edition, ChemTec Publishing, Ontario, 2016.

[7] F. Qiang, G. Wang, C. Liu, Polyethylene toughened by $CaCO_3$ particles: The interface behaviour and fracture mechanism in high density polyethylene/$CaCO_3$ blends, Polymer 36 (12) (1995) 2397–2401.

[8] M. Tolinski, Additives for polyolefins: getting the most out of polypropylene, polyethylene and TPO, William Andrew, Oxford, 2015.

[9] M. A. Osman, A. Atallah, Interparticle and particle–matrix interactions in polyethylene reinforcement and viscoelasticity, Polymer 46 (22) (2005) 9476–9488.

[10] S. C. Teixeira, M. M. Moreira, A. P. Lima, L. S. Santos, B. M. Da Rocha, E. S. De Lima, R. A. da Costa, A. L. N. da Silva, M. C. Rocha, F. M. Coutinho, Composites of high density polyethylene and different grades of calcium carbonate: mechanical, rheological, thermal, and morphological properties, Journal of Applied Polymer Science 101 (4) (2006) 2559–2564.

[11] S. Ersoy, M. Taşdemir, Zinc oxide (ZnO), magnesium hydroxide [$Mg(OH)_2$] and calcium carbonate ($CaCO_3$) filled HDPE polymer composites: Mechanical, thermal and morphological properties, Marmara Fen Bilimleri Dergisi 24 (4) (2012) 93–104.

[12] A. Lazzeri, S. M. Zebarjad, M. Pracella, K. Cavalier, R. Rosa, Filler toughening of plastics. part 1—the effect of surface interactions on physico-mechanical properties and rheological behaviour of ultrafine $CaCO_3$/HDPE nanocomposites, Polymer 46 (3) (2005) 827–844.

[13] C. Croitoru, A. Pascu, I. Roata, E. Stanciu, Obtaining and characterization of polyolefin-filled calcium carbonate composites modified with stearic acid, IOP Conference Series: Materials Science and Engineering 209 (1) (2017) 012041.

[14] C.-G. Ek, J. Kubát, M. Rigdahl, Stress relaxation, creep, and internal stresses in high density polyethylene filled with calcium carbonate, Rheologica Acta 26 (1) (1987) 55–63.

[15] A. Valadez-Gonzalez, J. Cervantes-Uc, L. Veleva, Mineral filler influence on the photo-oxidation of high density polyethylene: I. Accelerated UV chamber exposure test, Polymer Degradation and Stability 63 (2) (1999) 253–260.

[16] T. Zielinski, J. Kijenski, Plasma carbon black—the new active additive for plastics, Composites Part A: Applied Science and Manufacturing 36 (4) (2005) 467–471.

[17] T. M. Malik, P. J. Carreau, M. Grmela, A. Dufresne, Mechanical and rheological properties of carbon black filled polyethylene, Polymer Composites 9 (6) (1988) 412–418.

[18] F. Zuo, T. Finnegan, Light stabilization of polyethylene, in: A. Chatterjee, M. A. Spalding (Eds.), Handbook of Industrial Polyethylene and Technology, John Wiley & Sons, Inc., New Jersey, 2017, Ch. 26, pp. 772–788.

[19] J. Peña, N. Allen, M. Edge, C. Liauw, B. Valange, Interactions between carbon black and stabilisers in LDPE thermal oxidation, Polymer Degradation and Stability 72 (1) (2001) 163–174.

[20] J. Peña, N. Allen, C. Liauw, M. Edge, B. Valange, Factors influencing the adsorption of stabilizers onto carbon black: Flow microcalorimetry studies, Journal of Vinyl and Additive Technology 6 (2) (2000) 62–68.

[21] J. Peña, N. S. Allen, M. Edge, C. Liauw, B. Valange, Factors affecting the adsorption of stabilisers on to carbon black (flow micro-calorimetry studies) 4. Secondary antioxidants, Polymer Degradation and Stability 72 (1) (2001) 31–45.

[22] J. Peña, N. Allen, M. Edge, C. Liauw, O. Noiset, B. Valange, Factors affecting the adsorption of stabilisers on to carbon black (flow micro-calorimetry studies) Part II Hindered amine light stabilisers (HALS), Journal of Materials Science 36 (18) (2001) 4419–4431.

[23] J. Peña, N. Allen, M. Edge, C. Liauw, F. Santamaria, O. Noiset, B. Valange, Factors affecting the adsorption of stabilisers on to carbon black (flow micro-calorimetry and FTIR studies) Part I Primary phenolic antioxidants, Journal of Materials Science 36 (12) (2001) 2885–2898.

[24] G. Rideal, J. Padget, The thermal-mechanical degradation of high density polyethylene, Journal of Polymer Science: Polymer Symposia 57 (1) (1976) 1–15.

[25] J. J. Fay, R. E. King, III, Degradation and stabilization of polyethylene, in: A. Chatterjee, M. A. Spalding (Eds.), Handbook of Industrial Polyethylene and Technology, John Wiley & Sons, Inc., New Jersey, 2017, Ch. 25, pp. 754–768.

[26] J. L. Hodgson, M. L. Coote, Clarifying the mechanism of the Denisov cycle: how do hindered amine light stabilizers protect polymer coatings from photo-oxidative degradation?, Macromolecules 43 (10) (2010) 4573–4583.

[27] K. Menard, M. Noah, Thermal analysis of polyethylene, in: A. Chatterjee, M. A. Spalding (Eds.), Handbook of Industrial Polyethylene and Technology, John Wiley & Sons, Inc., New Jersey, 2017, Ch. 6, pp. 218–236.

[28] C.-Y. M. Tung, P. J. Dynes, Relationship between viscoelastic properties and gelation in thermosetting systems, Journal of Applied Polymer Science 27 (2) (1982) 569–574.

[29] D. Durand, M. Delsanti, M. Adam, J. Luck, Frequency dependence of viscoelastic properties of branched polymers near gelation threshold, Europhysics Letters 3 (3) (1987) 297.

[30] A. Dordinejad, F. Sharif, M. Ebrahimi, R. Rashedi, Time-sweep rheometry for evaluating polyethylene degradation behavior: Effect of formulation and process conditions, Polymer Testing 70 (2018) 39–46.

[31] G. W. Kamykowski, Rheology of polyethylene, in: A. Chatterjee, M. A. Spalding (Eds.), Handbook of Industrial Polyethylene and Technology, John Wiley & Sons, Inc., New Jersey, 2017, Ch. 7, pp. 240–280.

[32] J. A. Lee, M. Kontopoulou, J. S. Parent, Time and shear dependent rheology of maleated polyethylene and its nanocomposites, Polymer 45 (19) (2004) 6595–6600.

[33] P. A. Daly, D. A. Bruce, D. H. Melik, G. M. Harrison, Thermal degradation kinetics of poly (3-hydroxybutyrate-co-3-hydroxyhexanoate), Journal of Applied Polymer Science 98 (1) (2005) 66–74.

[34] J. D. Conrad, G. M. Harrison, The rheology and processing of renewable resource polymers, AIP Conference Proceedings 1027 (1) (2008) 114–116.

[35] M. Kruse, M. H. Wagner, Time-resolved rheometry of poly(ethylene terephthalate) during thermal and thermo-oxidative degradation, Rheologica Acta 55 (10) (2016) 789–800.

[36] P. Mariani, G. Carianni, D. Balducci, S. Roccasalvo, F. P. La Mantia, Melt stabilisation of high-density film-grade polyethylene, Macromolecular Symposia 176 (1) (2001) 73–82.

[37] P. Mariani, G. Carianni, F. Menconi, F. P. La Mantia, Correlation between processability and properties of a high density polyethylene by a rheological approach, Macromolecular Chemistry and Physics 203 (10-11) (2002) 1602–1605.

[38] R. Salehiyan, J. Bandyopadhyay, S. S. Ray, Mechanism of thermal degradation-induced gel formation in polyamide 6/ethylene vinyl alcohol blend nanocomposites studied by time-resolved rheology and hyphenated thermogravimetric analyzer Fourier transform infrared spectroscopy mass spectroscopy: synergistic role of nanoparticles and maleic-anhydride-grafted polypropylene, ACS Omega 4 (5) (2019) 9569–9582.

[39] B. Schroyen, J. W. Swan, P. Van Puyvelde, J. Vermant, Quantifying the dispersion quality of partially aggregated colloidal dispersions by high frequency rheology, Soft Matter 13 (43) (2017) 7897–7906.

[40] M. Mours, H. Winter, Time-resolved rheometry, Rheologica Acta 33 (5) (1994) 385–397.

[41] R. Salehiyan, T. Malwela, S. S. Ray, Thermo-oxidative degradation study of melt-processed polyethylene and its blend with polyamide using time-resolved rheometry, Polymer Degradation and Stability 139 (2017) 130–137.

[42] G. Filippone, S. Carroccio, R. Mendichi, L. Gioiella, N. T. Dintcheva, C. Gambarotti, Time-resolved rheology as a tool to monitor the progress of polymer degradation in the melt state–Part I: Thermal and thermo-oxidative degradation of polyamide 11, Polymer 72 (2015) 134–141.

[43] G. Filippone, S. Carroccio, G. Curcuruto, E. Passaglia, C. Gambarotti, N. T. Dintcheva, Time-resolved rheology as a tool to monitor the progress of polymer degradation in the melt state–Part II: Thermal and thermo-oxidative degradation of polyamide 11/organo-clay nanocomposites, Polymer 73 (2015) 102–110.

[44] D. W. Marquardt, R. D. Snee, Test statistics for mixture models, Technometrics 16 (4) (1974) 533–537.

[45] ASTM D3895 – 19, Standard test method for oxidative-induction time of polyolefins by differential scanning calorimetry, Standard, ASTM International, Philadelphia (2019).

[46] X. Hu, H. Xu, Z. Zhang, Influence of fillers on the effectiveness of stabilizers, Polymer Degradation and Stability 43 (2) (1994) 225–228.

[47] P. Jiangqing, X. Hongmei, Q. Juying, C. Jinfen, M. Zhenmin, Study of $CaCO_3$ filled polypropylene composite with long use life time, Polymer Degradation and Stability 33 (1) (1991) 67–75.

[48] N. S. Allen, E. Hoang, C. M. Liauw, M. Edge, E. Fontan, Influence of processing aids on the thermal and photostabilisation of HDPE with antioxidant blends, Polymer Degradation and Stability 72 (2) (2001) 367–376.

[49] A. J. Chirinos Padron, Performance and mechanisms of hindered amine light stabilizers in polymer photostabilization, Journal of Macromolecular Science—Reviews in Macromolecular Chemistry and Physics 30 (1) (1990) 107–154.

[50] M. A. Osman, A. Atallah, U. W. Suter, Influence of excessive filler coating on the tensile properties of LDPE–calcium carbonate composites, Polymer 45 (4) (2004) 1177–1183.

[51] T. Phease, N. Billingham, S. Bigger, The effect of carbon black on the oxidative induction time of medium-density polyethylene, Polymer 41 (26) (2000) 9123–9130.

[52] W. Hawkins, R. Hansen, W. Matreyek, F. Winslow, The effect of carbon black on thermal antioxidants for polyethylene, Journal of Applied Polymer Science 1 (1) (1959) 37–42.

[53] X. J. Bai, L. Wang, Effects of calcium carbonate on the thermal properties of acrylonitrile-butadiene-styrene/calcium carbonate composites, in: Advanced Materials Research, Vol. 834, Trans Tech Publ, 2014, pp. 276–280.

[54] C. D. C. Erbetta, G. F. Manoel, A. P. L. R. Oliveira, M. E. S. R. e Silva, R. F. S. Freitas, R. G. Sousa, Rheological and thermal behavior of high-density polyethylene (HDPE) at different temperatures, Materials Sciences and Applications 5 (13) (2014) 923.

[55] G. Socrates, Infrared and Raman Characteristic Group Frequencies, 3rd Edition, John Wiley & Sons, New Jersey, 2001.

[56] H.-J. Huang, Q.-B. Wang, B.-H. Xie, W. Yang, M.-B. Yang, Thermal oxidation and structural changes of degraded polyethylene in an oxygen atmosphere, Journal of Macromolecular Science, Part B 50 (7) (2011) 1376–1387.

[57] F. J. Stadler, H. Münstedt, Correlations between the shape of viscosity functions and the molecular structure of long-chain branched polyethylenes, Macromolecular Materials and Engineering 294 (1) (2009) 25–34.